Naval Research Laboratory

Washington, DC 20375-5320

NRL/MR/6730--20-10,054

Machining Inertial Confinement Fusion Relevant Isolated Defects in Polystyrene Foils (Isolated Defects)

Calvin Zulick
Steve Obenschain

Laser Plasma Branch
Plasma Physics Division

February 14, 2020

REPORT DOCUMENTATION PAGE

Form Approved
OMB No. 0704-0188

1. REPORT DATE *(DD-MM-YYYY)*	**2. REPORT TYPE**	**3. DATES COVERED** *(From - To)*
14-02-2020	NRL Memorandum Report	June 2018 – June 2019

4. TITLE AND SUBTITLE

Machining Inertial Confinement Fusion Relevant Isolated Defects in Polystyrene Foils (Isolated Defects)

5a. CONTRACT NUMBER

5b. GRANT NUMBER

5c. PROGRAM ELEMENT NUMBER
NISE

6. AUTHOR(S)

Calvin Zulick and Steve Obenschain

5d. PROJECT NUMBER

5e. TASK NUMBER

5f. WORK UNIT NUMBER
N2P7

7. PERFORMING ORGANIZATION NAME(S) AND ADDRESS(ES)

Naval Research Laboratory
4555 Overlook Avenue, SW
Washington, DC 20375-5320

8. PERFORMING ORGANIZATION REPORT NUMBER

NRL/MR/6730--20-10,054

9. SPONSORING / MONITORING AGENCY NAME(S) AND ADDRESS(ES)

Naval Research Laboratory
4555 Overlook Avenue, SW
Washington, DC 20375-5320

10. SPONSOR / MONITOR'S ACRONYM(S)

NRL-NISE

11. SPONSOR / MONITOR'S REPORT NUMBER(S)

12. DISTRIBUTION / AVAILABILITY STATEMENT

DISTRIBUTION STATEMENT A: Approved for public release distribution is unlimited.

13. SUPPLEMENTARY NOTES

Karles Fellowship

14. ABSTRACT

Research was performed to study the hydrodynamic growth of instabilities seeded by isolated perturbations in targets ablatively accelerated to high velocity. Experiments were performed on the NIKE laser facility at the Naval Research Laboratory (NRL) which led to improved understanding of isolated perturbation growth and provided a comprehensive data set for simulations by advanced hydrocodes such as NRLs FASTRAD3D. Isolated defects were machined into 40 um polystyrene foils using the NRL femtosecond Swept-Wavelength Optical Resonance-Raman Device (SWOrRD). Isolated defects where characterized with microscopy and white light interferometry. This memorandum summarizes the machining results of this research effort.

15. SUBJECT TERMS

Laser machining

16. SECURITY CLASSIFICATION OF:			**17. LIMITATION OF ABSTRACT**	**18. NUMBER OF PAGES**	**19a. NAME OF RESPONSIBLE PERSON**
a. REPORT	**b. ABSTRACT**	**c. THIS PAGE**			Calvin Zulick
Unclassified Unlimited	Unclassified Unlimited	Unclassified Unlimited	Unclassified Unlimited	14	**19b. TELEPHONE NUMBER** *(include area code)* (202) 404-3879

Standard Form 298 (Rev. 8-98)
Prescribed by ANSI Std. Z39.18

This page intentionally left blank.

CONTENTS

FIGURES

EXECUTIVE SUMMARY

Research was performed to study the hydrodynamic growth of instabilities seeded by isolated perturbations in targets ablatively accelerated to high velocity. Experiments were performed on the NIKE laser facility at the Naval Research Laboratory (NRL) which led to improved understanding of isolated perturbation growth and provided a comprehensive data set for simulations by advanced hydrocodes such as NRLs FASTRAD3D. Isolated defects were machined into 40 μm polystyrene foils using the NRL femtosecond Swept-Wavelength Optical Resonance-Raman Device (SWOrRD). Isolated defects where characterized with microscopy and white light interferometry. This memorandum summarizes the machining results of this research effort.

The results of 86 machined grooves are reported. Groove dimensions ranged from 100 nm to 25 μm deep by 1 μm to 30 μm wide. It was possible to make shallow grooves, with aspect ratios of 1 : 10, but more difficult to make deep cuts, which were limited to aspect ratios of 2 : 1. Groove width was primarily determined by the optics and the pulse energy, while groove depth was tailored by increasing or decreasing the number of laser pulses per unit distance, or line density. Groove uniformity was observed to improve with groove depth which was attributed statistical smoothing as a result of the increased number of laser pulses required to etch deeper into the material.

This page intentionally left blank.

MACHINING INERTIAL CONFINEMENT FUSION RELEVANT ISOLATED DEFECTS IN POLYSTYRENE FOILS

1. BACKGROUND

Plasma instabilities, i.e. Richtmyer-Meshkov and Rayleigh-Taylor, are seeded in non-uniform targets and undergo hydrodynamic growth during ablative acceleration. In Inertial Confinement Fusion (ICF) these perturbations can lead to asymmetric target compression and mixing of the ablator material into the fuel [1]. Previous efforts to understand perturbation growth have largely focused on studies of uniformly imposed 2-D structures such as sinusoidal modulations in the surface of targets [2, 3]. However, several sources of 3-D isolated perturbations, including fill tubes, mounting support structures, pits, and other surface flaws, have recently been identified as significant obstacles on the path toward ignition for indirect drive on the National Ignition Facility [4–7]. Similar effects are expected for direct laser drive, which is primarily advanced by the University of Rochester and NRL [8]. A better understanding of instability growth rates, as well as the associated mechanisms leading to the formation of high velocity plasma jets around isolated perturbations, are necessary to better understand and mitigate instability growth.

1.1 Scientific Goals

A combination of experiments and simulations are required to advance our understanding of isolated perturbation growth. The work focused on studies of hydrodynamic instabilities seeded by isolated grooves in the targets. The primary experimental diagnostics were face-on and side-on x-ray radiography, as shown in Fig. 1. Time resolved face-on measurements were acquired by imaging x-rays, transmitted through the target from an x-ray backlighting source, onto a streak camera. This diagnostic provided a measurement of the evolution of the areal density across the width of the isolated defect, allowing measurement of the width, depth, and growth rates of the perturbation over a 5 ns time window.

The side-on diagnostic measured a 2-D spatial image of x-rays transmitted along the target surfaces onto image plate. This provided a snapshot of the two dimensional structure of the foil by using a > 500 ps duration backlighter of which the time delay, relative to the main pulse, could be varied. By combining these images with the streaked areal density it was possible to match specific features in the streaked image to two-dimensional structures in the foil.

This experimental data was analyzed to evaluate growth rates, as a function of initial perturbation size, and compared to FASTRAD3D simulations. Out-of-plane perturbation closure, on the front side of the target, and jets, on the rear side of the target, were observed experimentally and in simulations, providing a valuable tool for validation of the hydrocode. These results are currently in preparation for publication.

1.2 Technical Approach

ICF targets are generally single shell spheres with diameters of about a millimeter and shell thicknesses of about 100 um. As a result, ICF-relevant feature sizes of range from 100's of nm to an upper limit of a few

Manuscript approved September 23, 2019.

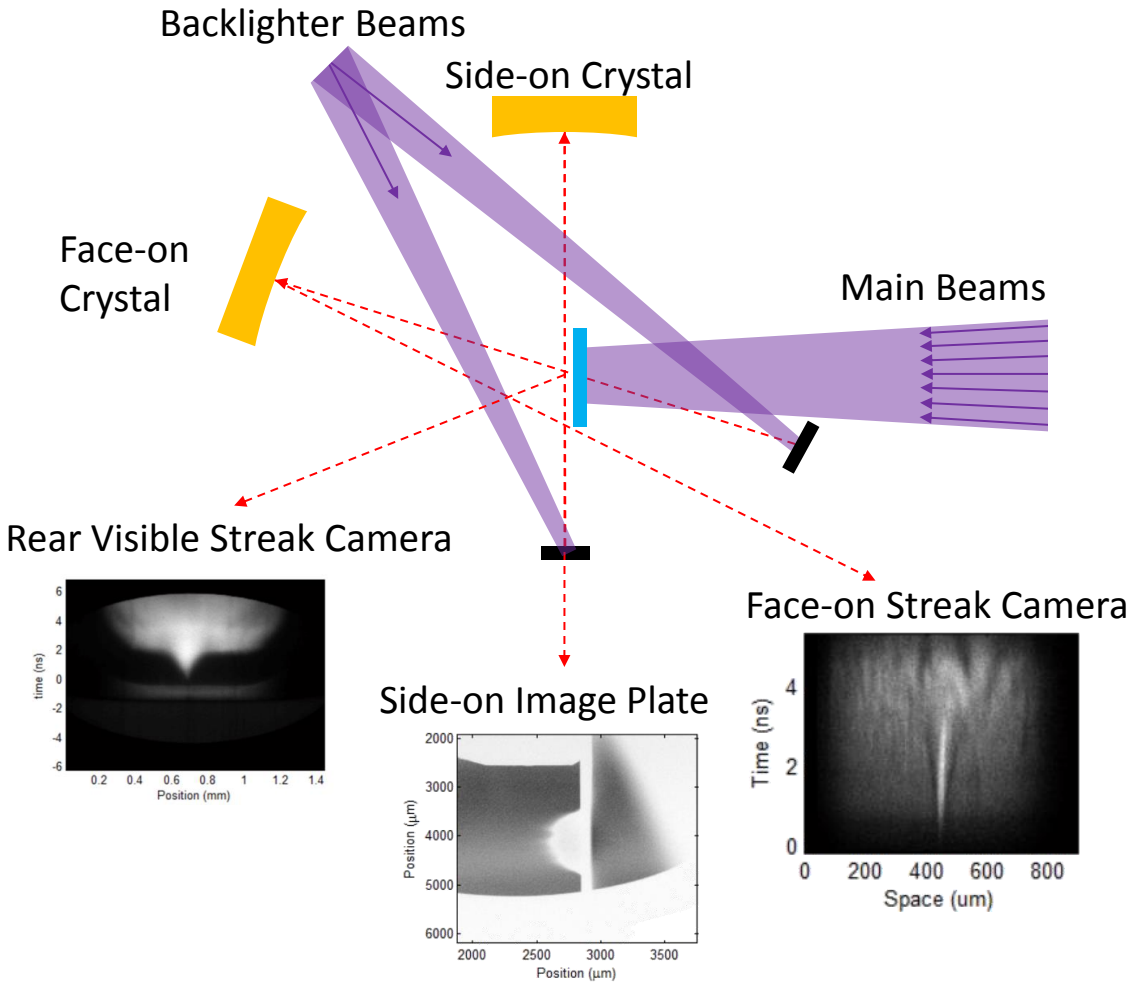

Fig. 1 — Experimental setup of isolated defect experiment on NIKE laser showing main and backlighter beam alignment as well as face-on and side-on imaging crystal configuration. Example images of the collected data are also shown for each diagnostic.

10's of μm, as larger defects approach the shell thickness. Machining defects of this size in frail foils requires delicate and precision machining techniques. Additionally, hydrodynamic shocks can be significantly altered by changes in material densities and non-uniformities which produce material interfaces, changing the shock velocity and producing reflections. Thus, it was preferable to machine the target in a way that did not heat the area surrounding the defect, avoiding density and phase changes.

Laser machining with femtosecond duration pulses provided a platform capable of creating the desired defects while avoiding target heating. This was possible because, as an optical technique utilizing visible wavelength light, feature sizes of hundreds of nanometers to tens of microns are comparable to the optical wavelength and therefor easily achievable. Additionally, femtosecond lasers interact with materials by interacting primarily with electrons, stripping them out of their atoms and ionizing the material, leading to expulsion of ionized material from the laser focus. This interaction occurs over time scales that were short enough to prevent the transfer of significant energy from the laser to the heavier ions, avoiding significant

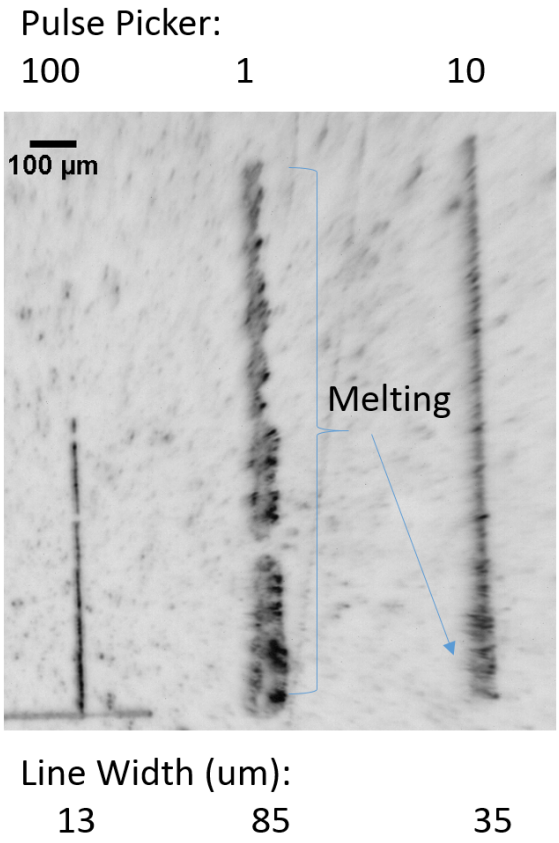

Fig. 2 — Varying pulse picker rates, 1 : 1, 1 : 10, and 1 : 100, were used to change the time averaged energy deposition and material ablation rate. Melting, resulting in increased cut width and the formation of bubbles, was evident at full repetition rate (pulse picker = 1), and at the bottom of the cut for a pulse picker of 1 : 10. No melting was observed with a pulse picker of 1 : 100.

heating of the material. The spatial threshold for ionization of the target, which was a function of both the material properties and the laser profile, was also well defined, allowing precise machining of material. One last benefit of this technique was that femtosecond laser systems are typically intrinsically high repetition rate (MHz) and it was practical to achieve amplified laser pulses at ionizing intensities with repetition rates in excess of kHz. This allowed optical machining to be done with a large number of pulses, reducing machining variations through statistical means.

The work was performed using the femtosecond version of the SWOrRD laser at NRL [9], with laser parameters as shown in Table 1. The laser utilizes an optical parametric amplifier (OPA) and multiple frequency conversion crystals to convert 1030 nm light from the Yb:KGW oscillator into wavelengths ranging from 210 nm to 2.6 μm. The OPA signal beam was used at 690 nm for this experiment, which was close to the maximum pulse energy (at 670 nm). Shorter wavelengths could have produced smaller diffraction limited focal spots, however there were significant energy losses as a result of frequency conversion and lower reflectivity and transmission of optics, in particular the microscope objective used to focus the light on target.

At full repetition rate, 250 kHz, the time averaged power on target was sufficient ($>$ 10's of mW) to melt the target material. Two adjustments were performed to keep the time averaged power below the melting threshold. First, a pulse picker was utilized to select a fraction of the pulses, typically 1 in 10, dropping the effective repetition rate to 25 kHz. Second, the second harmonic crystal which produced the 515 nm pump beam for the OPA was detuned to reduce the efficiency of the OPA process. Both of these adjustments maintained the pulse temporal and spatial profile, allowing uniform and repeatable machining while varying the pulse power to achieve sufficient ablation of material during the machining process. Fig. 2 shows the results of cuts with different pulse picker settings, ranging form 1 : 1 (all pulses) to 1 : 100 (one out of a hundred pulses). Melting was observed for the entire length of the PP = 1 cut. Melting was also observed on the bottom of the PP = 10 cut, which was the result of slower transversal movement of the target foil during the etching, allowing heat to build up.

Both a 5x objective and a 40x objective were used. The the 40x objective provided a tighter focus and finer machining control, while the lower magnification objective provided deeper cuts, as a result of the longer Rayleigh range. The objectives were mounted in a microscope and a partially reflecting mirror was used to provide simultaneous imaging and machining of the target. The targets were mounted on a two axis stage with micrometer adjustment dials allowing $\approx$ micron accuracy when coupled with the high resolution optical microscope. The dials were turned by hand which resulted in variable transversal speeds which negatively impacted the uniformity of the grooves. All grooves were machined 500 μm long. This length was chosen to allow targets to be etched with up to three grooves, each separated by 150 μm, while keeping the entirety of the grooves within the NIKE laser 750 μm flat-top focal spot.

Table 1 — SWOrRD Laser Parameters.

Parameter	Value
Repetition Rate	250 kHz
Pulse Length	280 fs
Pulse Energy at 1030 nm	40 μJ
Pulse Energy at 700 nm	Up to 2 μJ
Average Power at 700 nm	Up to 500 mW
Intensity at 1030 nm	$< 10^{14}$ W/cm^2

A Zygo NewView 5000 white light interferometer [10] was used to precisely characterize the targets after machining. White light interferometry, and specifically this device, was capable of constructing a $3D$ surface profile of the target with sub-nm resolution as long as the target was smooth enough that there were not issues with the data recovery algorithm as a result of multiple fringe shifts from large discontinuities.

1.3 Results

A plot of the dimensions of 86 grooves machined as part of this experimental effort is shown in Fig. 3. Several methods were tested for varying the width and depths of grooves. One optical approach was to change the focusing optic from a 5x objective to a 40x objective. The sharper focus, or equivalently, smaller f/#, of the 40x objective focused the light down to a smaller focal diameter, increasing the laser intensity ($I = W cm^{-2}$), and decreasing the distance over which the Gaussian beam maintains a focal diameter within a factor of $\sqrt{2}$, also known as the Rayleigh length ($z_R = \frac{\pi\omega_0^2}{\lambda}$ where ω_0 is the beam waist at focus).

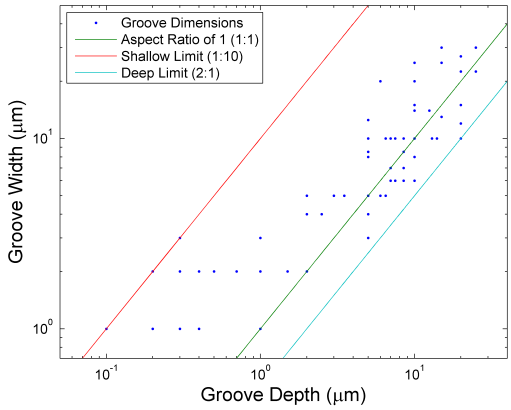

Fig. 3 — Scatter plot of the dimensions of 86 machined grooves. Lines are plotted to show aspect ratios of the shallow limit (1 : 10), the deep limit (2 : 1), and an aspect ratio of 1 (1 : 1).

This allowed machining of smaller features with less laser power and limited the cut depth due to faster defocusing.

The most effective method of changing the cut depth, without changing the width, was repeating the cut, i.e. passing over the same area multiple times with the laser and changing the focal depth as necessary. Fundamentally, this increased the cut depth by increasing the number of shots and thus the amount of material ablated from the groove without changing the shape or intensity of the laser pulse. This approach also allowed the focal depth to be optimized between passes keeping the bottom of the cut within the Rayleigh range. This approach was superior to alternative methods of increasing the shot line density such as increasing the laser repetition rate or the exposure time by moving the target at a slower rate. This was likely due to the deleterious effects of increased heating of the target, while the multi-pass approach allowed the cut area to cool between passes. Fig. 4 shows the results of cuts using multiple passes over the same section of the target, as well as two power levels. At attenuated power the use of multiple passes increased the cut depth from 200 nm to 3 μm while only increasing the width from 4 to 7 μm. Alternatively, the grooves machined at full power increased primarily in width with additional passes. This was likely because the increased power, at the same pulse picker setting, resulted in the full groove depth being etched on the first pass while subsequent passes only increased the width of the cut.

The cut width was primarily determined by the focal spot diameter, which was determined by the focusing optic and the pulse power. As the power increased the diameter of the focal spot which was above the ionization threshold intensity ($\approx 10^{12} W cm^{-2}$) also grew, and therefore increased the width of the cut. It was possible to cut grooves with much smaller depths than widths (1 : 10) as shown by the red line in Fig. 3. However, deep cuts with narrow widths were limited to aspect ratios of about 2 : 1, as shown by the blue line. This was likely a result of the combination of optical effects, such as diffraction of light off the edge of the grooves, and ballistic considerations of the ablated material, preventing ablated material from leaving the groove.

Images of the center portion of two machined grooves are shown in Fig. 5 and Fig. 6. Fig. 5 shows a 1 x 1 μm groove (a) along with a lineout (b) that shows the profile of the cut. This measurement also shows that

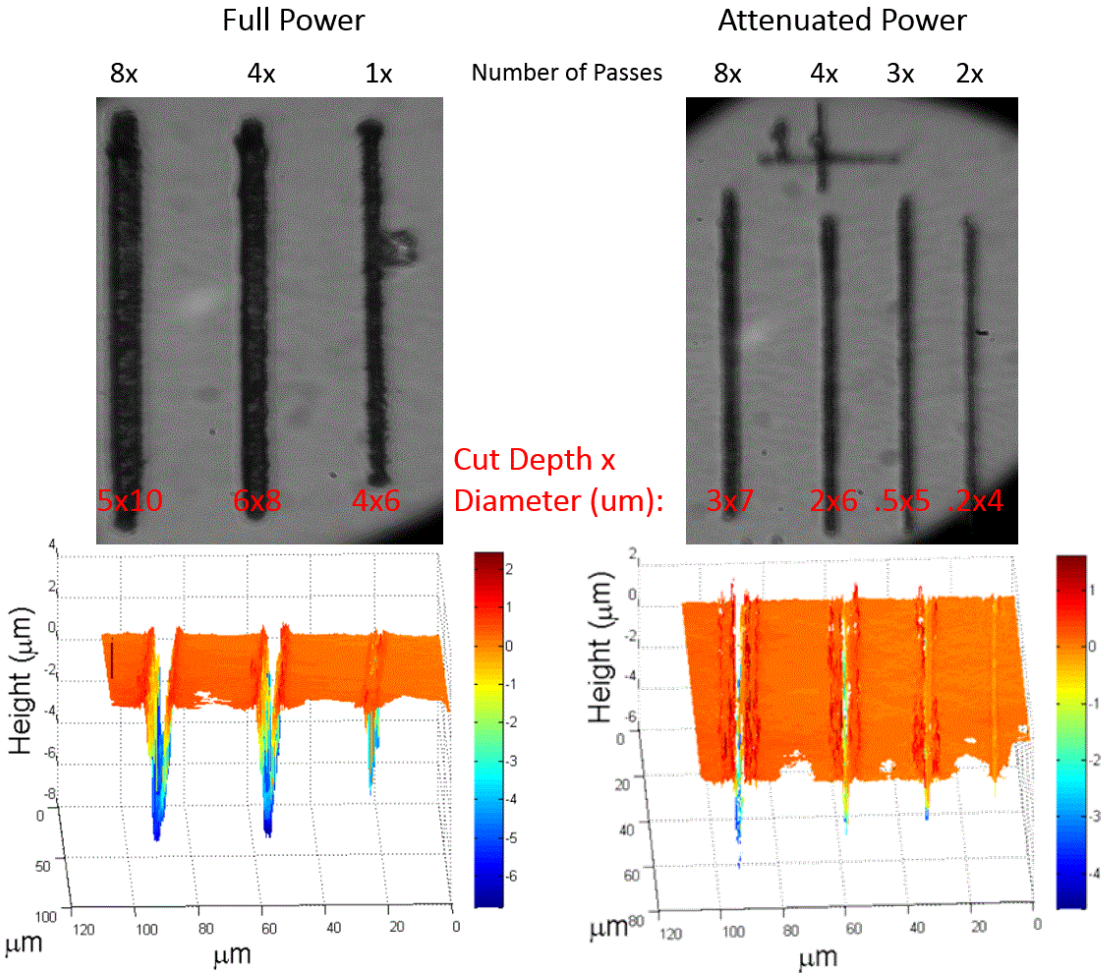

Fig. 4 — Grooves were machined into 30 μm polystyrene using two power levels and multiple passes over the same area of the target. Subsequent passes resulted in substantially deeper cuts with somewhat increased widths for the attenuated power cuts.

the area around the cut was unperturbed, as desired, however there was some variation in the depth of the cut along the length of the groove. This variation was reduced on deeper cuts that involved multi-pass etching, which reduced the statistical variation of the cut depth. Fig. 6 shows a much larger cut 10 x 8 μm, which had a more uniform depth. Interferometry measurements of grooves with similar or larger depths typically produced sparse measurements of the bottom of the grooves due to the large discontinuity and the roughness of the etched material. However, the uniformity and shape of the cut was evident during the measurement process as a result of speckle interference from the bottom of the cut, which was visible by eye but was not recovered by the instrument's analysis algorithm. Larger cuts also exhibited a small ridge of material along the edges of the groove. This was observed to have a height of $\approx 1/10$th of the depth of the groove, and a width of $1/2$ to $1/4$ of the width of the groove. The material appeared to be debris that had been ablated out of the groove and no etching method was determined to avoid the formation of ridges on large cuts. Fortunately, the scale of the ridge was small enough that it was judged to have minimal potential for impact on the experimental measurements.

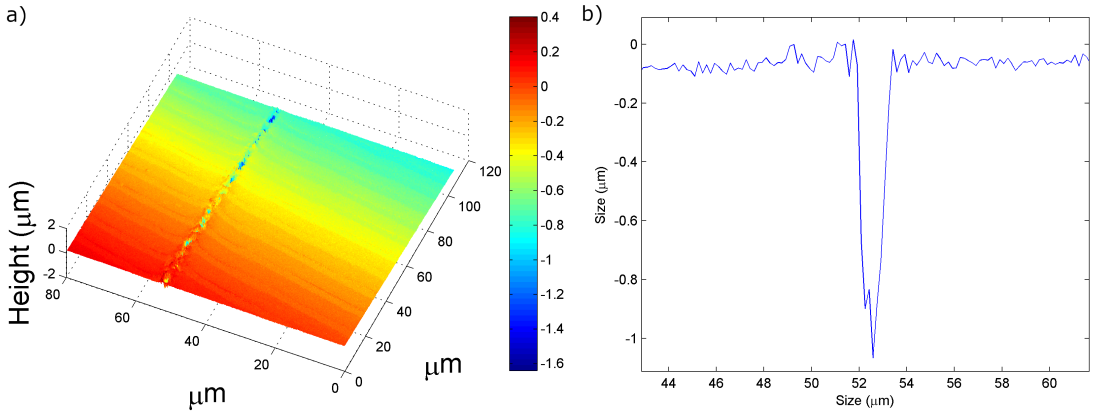

Fig. 5 — White light interferometry image of a 1 x 1 μm groove.

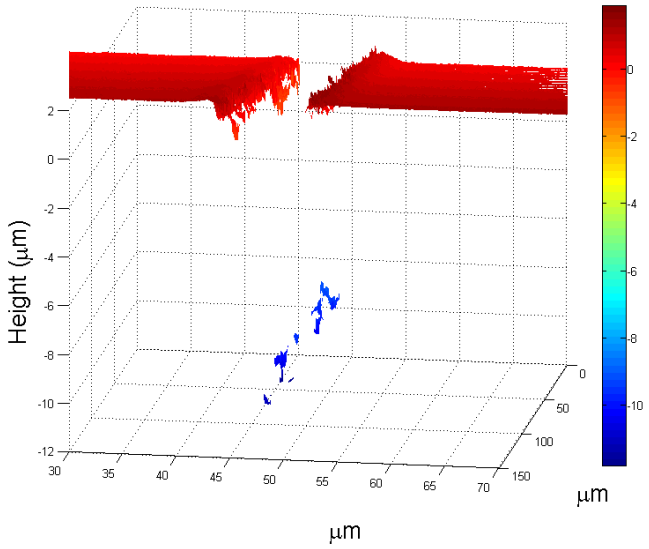

Fig. 6 — White light interferometry image of a 10 x 8 μm groove.

1.4 Conclusions

Research was performed to study the hydrodynamic growth of instabilities seeded by isolated perturbations in targets ablatively accelerated to high velocity. Experiments were performed on the NIKE laser facility at the Naval Research Laboratory (NRL) which led to improved understanding of isolated perturbation growth and provided a comprehensive data set for simulations by advanced hydrocodes such as NRLs FASTRAD3D. Isolated defects were machined into 40 μm polystyrene foils using the NRL femtosecond Swept-Wavelength Optical Resonance-Raman Device (SWOrRD). Isolated defects where characterized

with microscopy and white light interferometry. This memorandum summarizes the machining results of this research effort.

The results of 86 machined grooves are reported. Groove dimensions ranged from 100 nm to 25 μm deep by 1 μm to 30 μm wide. It was possible to make shallow grooves, with aspect ratios of 1 : 10, but more difficult to make deep cuts, which were limited to aspect ratios of 2 : 1. Groove width was primarily determined by the optics and the pulse energy, while groove depth was tailored by increasing or decreasing the number of laser pulses per unit distance, or line density. Groove uniformity was observed to improve with groove depth which was attributed statistical smoothing as a result of the increased number of laser pulses required to etch deeper into the material.

Future efforts will evaluate the impact of changing wavelengths, primarily to shorter wavelengths. The SWOrRD laser should have enough power to machine at shorter wavelengths despite losses from the harmonic conversion process. Additionally, automation of the target holding motion stage is expected to improve reproducibility of cuts and allow more complicated designs as well as a systematic investigation of target movement, or shot line density, rates and the impact on the quality of the cut.

ACKNOWLEDGMENTS

This research was supported by a Naval Research Laboratory Karles Fellowship. The SWOrRD femtosecond laser was purchased with code 6700 CPP funding.

REFERENCES

1. A. B. Zylstra, S. MacLaren, S. A. Yi, J. Kline, D. Callahan, O. Hurricane, B. Bachmann, G. Kyrala, L. Masse, P. Patel, J. E. Ralph, J. Salmonson, P. Volegov, and C. Wilde, "Implosion performance of subscale beryllium capsules on the nif," *Physics of Plasmas* **26**(5), 052707 (2019), doi: 10.1063/1.5098319, URL https://doi.org/10.1063/1.5098319.

2. G. Dimonte, P. Ramaprabhu, D. L. Youngs, M. J. Andrews, and R. Rosner, "Recent advances in the turbulent rayleightaylor instability," *Physics of Plasmas* **12**(5), 056301 (2005), doi: 10.1063/1.1871952, URL https://doi.org/10.1063/1.1871952.

3. G. Dimonte, D. L. Youngs, A. Dimits, S. Weber, M. Marinak, S. Wunsch, C. Garasi, A. Robinson, M. J. Andrews, P. Ramaprabhu, A. C. Calder, B. Fryxell, J. Biello, L. Dursi, P. MacNeice, K. Olson, P. Ricker, R. Rosner, F. Timmes, H. Tufo, Y.-N. Young, and M. Zingale, "A comparative study of the turbulent rayleightaylor instability using high-resolution three-dimensional numerical simulations: The alpha-group collaboration," *Physics of Fluids* **16**(5), 1668–1693 (2004), doi: 10.1063/1.1688328, URL https://doi.org/10.1063/1.1688328.

4. A. G. MacPhee, D. T. Casey, D. S. Clark, S. Felker, J. E. Field, S. W. Haan, B. A. Hammel, J. Kroll, O. L. Landen, D. A. Martinez, P. Michel, J. Milovich, A. Moore, A. Nikroo, N. Rice, H. F. Robey, V. A. Smalyuk, M. Stadermann, and C. R. Weber, "X-ray shadow imprint of hydrodynamic instabilities on the surface of inertial confinement fusion capsules by the fuel fill tube," *Phys. Rev. E* **95**, 031204 (Mar 2017), doi: 10.1103/PhysRevE.95.031204, URL https://link.aps.org/doi/10.1103/PhysRevE.95.031204.

5. A. G. MacPhee, V. A. Smalyuk, O. L. Landen, C. R. Weber, H. F. Robey, E. L. Alfonso, K. L. Baker, L. F. Berzak Hopkins, J. Biener, T. Bunn, D. T. Casey, D. S. Clark, J. W. Crippen, L. Divol, M. Farrell, S. Felker, J. E. Field, W. W. Hsing, C. Kong, S. Le Pape, D. A. Martinez, P. Michel, J. Milovich, A. Moore, A. Nikroo, L. Pickworth, N. Rice, M. Stadermann, C. Yeamans, and C. Wild, "Hydrodynamic instabilities seeded by the x-ray shadow of icf capsule fill-tubes," *Physics of Plasmas* **25**(7), 072705 (2018), doi: 10.1063/1.5042081, URL https://doi.org/10.1063/1.5042081.

6. S. R. Nagel, S. W. Haan, J. R. Rygg, M. Barrios, L. R. Benedetti, D. K. Bradley, J. E. Field, B. A. Hammel, N. Izumi, O. S. Jones, S. F. Khan, T. Ma, A. E. Pak, R. Tommasini, and R. P. J. Town, "Effect of the mounting membrane on shape in inertial confinement fusion implosions," *Physics of Plasmas* **22**(2), 022704 (2015), doi: 10.1063/1.4907179, URL https://doi.org/10.1063/1.4907179.

7. V. A. Smalyuk, C. R. Weber, H. F. Robey, D. T. Casey, K.-C. Chen, D. S. Clark, M. Farrell, S. Felker, J. E. Field, S. W. Haan, B. A. Hammel, A. V. Hamza, D. Hoover, J. J. Kroll, O. L. Landen, A. G. MacPhee, D. Martinez, A. Nikroo, and N. Rice, "Hydrodynamic instability growth of three-dimensional modulations in radiation-driven implosions with low-foot and high-foot drives at the national ignition facility," *Physics of Plasmas* **24**(4), 042706 (2017), doi: 10.1063/1.4980002, URL https://doi.org/10.1063/1.4980002.

8. I. Igumenshchev, F. Marshall, J. Marozas, V. Smalyuk, R. Epstein, V. Goncharov, T. Collins, T. Sangster, and S. Skupsky, "The effects of target mounts in direct-drive implosions on omega," *Physics of Plasmas* **16**(8), 082701 (2009).

9. J. Grun, C. K. Manka, S. Nikitin, D. Zabetakis, G. Comanescu, D. Gillis, and J. Bowles, "Identification of bacteria from two-dimensional resonant-raman spectra," *Analytical Chemistry* **79**(14), 5489–5493 (2007), doi: 10.1021/ac070681h, URL https://doi.org/10.1021/ac070681h, PMID: 17559190.

10. J. C. Wyant, "White light interferometry," in *Holography: A Tribute to Yuri Denisyuk and Emmett Leith*, volume 4737, pp. 98–107 (International Society for Optics and Photonics, 2002).